Fusion Engineering and Design 173 (2021) 112860

Contents lists available at ScienceDirect

Fusion Engineering and Design

journal homepage: www.elsevier.com/locate/fusengdes

Analysis of supercritical carbon dioxide Brayton cycles for a helium-cooled pebble bed blanket DEMO-like fusion power plant

J. Hidalgo-Salaverri [a,b,c,*], P. Cano-Megias [a,b], R. Chacartegui [b], J. Ayllon-Guerola [a,c], E. Viezzer [a,d]

[a] CNA (Universidad de Sevilla, CSIC, J. de Andalucía), C/ Tomás Alva Edison 7, 41092, Sevilla, España
[b] Dpto Ingeniería Energética, Escuela Técnica Superior de Ingeniería, Universidad de Sevilla, Camino de los Descubrimientos s/n, 41092 Sevilla, Spain
[c] Dpto de Ingeniería Mecánica y Fabricación, Escuela Técnica Superior de Ingeniería, Universidad de Sevilla, Camino de los Descubrimientos s/n, 41092 Sevilla, Spain
[d] Dpto de Física Atómica, Molecular y Nuclear, Facultad de Física, Universidad de Sevilla, Avda. de la Reina Mercedes s/n, 41012 Sevilla, Spain

ARTICLE INFO

Keywords:
Balance Of Plant (BOP)
PROCESS
Supercritical carbon dioxide (S-CO_2) Brayton cycle
EU-DEMO nuclear fusion power plant
Thermal Energy Storage (TES)

ABSTRACT

Nuclear fusion is expected to be a clean and almost-unlimited power source in the near future. The first net power demonstration plant (DEMO) is planned to start operation in 2050. The supercritical carbon dioxide (S-CO_2) Brayton cycle is an excellent candidate for integration with a fusion power plant, such as DEMO, because of its high efficiency at intermediate temperatures and low interaction of coolant with tritium.

This work analyses a set of S-CO_2 Brayton cycle layouts for its integration in a DEMO-like fusion power plant, considering the specific requirements and heat availability characteristics. A framework has been developed to integrate the PROCESS code and the numerical solver EES to study the thermal and economic aspects of integrating the different S-CO_2 cycle layouts. In total, 14 layouts have been studied and grouped into a more conservative (DEMO1, pulsed operation) and more advanced (DEMO2, steady-state operation) fusion reactors. The PROCESS code has been used to obtain the DEMO 2018 Baseline, which defines the available power from each heat source and their boundary conditions. This code has also been used to assess the cost of the optimal layout. Thermal storage has been added to the DEMO1 scenario to avoid standby times that could negatively affect the cycle equipment lifetime and efficiency. Besides, these boundary conditions have been extended to account for possible technical improvements by the time of its construction in the DEMO2 scenario.

A sensitivity analysis of the most characteristic parameters of the cycles shows a strong dependence on the turbine inlet temperature for all layouts, which is constrained by the reactor material limits. The cycle efficiency (electric power produced before consumptions non-related to the cycle) has been selected as the figure of merit for the optimisation. The results show a 38% cycle efficiency for DEMO1 and 56% for DEMO2 scenarios. These efficiencies drop to 20% and 38% values, respectively, when the reactor and cooling loop power consumptions are considered. These values are obtained for current fusion reactor conceptual designs. The economic analysis shows the economic viability of DEMO2 scenarios.

1. Introduction

The energy market is currently immersed in a decarbonisation stage. Nuclear fusion is a clean, safe and almost unlimited energy source, which constitutes an excellent candidate to participate in the new energy mix. The expected displacement of carbon-based power production will open the door for new baseload producers, with large production capacity, as nuclear fusion power plants. The European Fusion Roadmap [1] determines the implementation of fusion power plants in Europe. The next crucial milestone in this pathway is the construction of the international ITER project. The ITER project, currently under construction in Cadarache (France), is meant to demonstrate the capability of achieving net thermal power from a fusion reactor based on a magnetic confinement device. In parallel, different countries and international bodies are working on the design and construction of pilot fusion power plants. The EU DEMO reactor will tackle this task in the European Roadmap by 2050 as the first demonstration of net electric fusion power fed into the electric grid [1]. This milestone is expected to open the pathway for constructing commercial power plants based on nuclear fusion.

DEMO is intended as a prototype of a commercial fusion power plant

* Corresponding author.

https://doi.org/10.1016/j.fusengdes.2021.112860
Received 27 May 2021; Received in revised form 14 August 2021; Accepted 1 September 2021
Available online 13 September 2021

Nomenclature

S-CO_2	Supercritical carbon dioxide
TES	Thermal Energy Storage
SHS	Sensible Heat Storage
PCM	Phase-Change Materials
TCES	Thermochemical Energy Storage
LCOE	Levelized Cost Of Electricity
EFDA	European Fusion Development Agreement
WCLL	Water-Cooled Lithium-Lead blanket
HCLL	Helium-Cooled Lithium-Lead blanket
HCPB	Helium-Cooled Pebble Bed blanket
BNK	Blanket and first wall heat source
DIV	Divertor heat source
SHD	Shield heat source
LTR	Low-Temperature Recuperator
HTR	High-Temperature Recuperator
TD	Temperature Difference
HLC	HTR-LTR-secondary compressor high-pressure side layout
HCL	HTR-secondary compressor- LTR high-pressure side layout
NC	No secondary compressor high-pressure side layout
α	Mass fraction flowing through the secondary compressor
DSL	DIV-SHD-LTR low-pressure side layout
LDS	LTR-DIV-SHD low-pressure side layout
NDS	No DIV and SHD low-pressure side layout
HT	High Temperature
SS	Steady-state
2T	Double turbine
HRF	Heat Recovery Fraction

and as the last step in the research-focused reactors [1]. Its main goal is to produce electric power, but not to compete with the other energy agents in the electric market. Lessons learnt from ITER and DEMO will play a significant role in the commercial reactors that will follow DEMO. In this work, a power plant based on DEMO is studied to explore the reference design and to discern what paths should be followed to improve future fusion power plants designs.

The deuterium-tritium fusion reaction is the best candidate as it has the largest cross-section at relatively low input energy. Deuterium is easily obtainable as it can be found in seawater. However, tritium is a radioactive material with a very short half-life of 12.3 years, so natural reserves are almost non-existent. DEMO will self-supply its tritium consumption through the addition of a breeding blanket. This breeding blanket consists of a layer of lithium that will receive the impact of the neutrons exiting the plasma. The resulting nuclear reaction produces tritium. DEMO will be the first fusion experiment to feature a complete breeding blanket. ITER will only have a limited breeding blanket for testing purposes [2].

The fusion reactor will be integrated with a power conversion system to generate electricity from the thermal power [3,4]. Different cycles have been proposed to fulfil this role, such as a Rankine cycle [5], with an estimated efficiency of 37.7%, and requiring large installations, or a Helium Brayton cycle [6], with an efficiency of 37%. It is relevant to highlight that the assumptions regarding the design and boundary conditions of the DEMO project will change in time as its design gets more refined in the iterative design process. Comparisons amongst existing studies must consider these differences in the designs and contributions are required in this pathway.

The supercritical carbon dioxide (S-CO_2) Brayton cycle or Feher cycle [7] was first presented by Sulzer Bros in 1948 [8]. Supercritical carbon dioxide cycles are characterised by excellent efficiencies for medium-range temperatures, relatively small machinery and little power consumption in the compressor as it is working close to the critical point [9,10]. The S-CO_2 Brayton cycle has been proposed for concentrated solar power in [9,11], where it compared positively with other technologies. In [12], the effect of varying thermal power input in a solar-thermal power plant is studied, concluding that the thermal inertia of the system can overcome short power outages. In [13], this cycle is used in a biomass-fired oxy-combustion power plant instead of a conventional Rankine cycle to reduce costs and increase the cycle efficiency. An S-CO_2 Brayton cycle for a 1000 MW coal power plant is presented in [14], achieving an overall power plant efficiency of 50%. In [15], a state-of-the-art review of the different cycles available in the literature is presented and reaffirms the wide range of applications of the S-CO_2 Brayton cycle. Wu et al. [16] reviews the advantages of this cycle for various nuclear power plants applications, proposing its usage in small nuclear reactors, generation IV nuclear fission power plants and fusion power plants.

S-CO_2 Brayton cycles have also been proposed as the power conversion system associated with a future DEMO-like reactor [2,4,5]. Linares et al. [17] proposes a series of cycles based on an S-CO_2 Brayton cycle with a double recuperator and double compressor. In these layouts, heat coming from the breeding blanket is always included before entering the turbine. The power from secondary heat sources is, in some cases, included in a channel that by-passes the low-temperature recuperator or at the secondary compressor outlet. Vesely et al. [18] studied a double recuperator, double compressor layout with only the input from the breeding blanket. In [18], a double recuperator, single compressor layout is also studied, where the rest of the heat sources are used in parallel to the low-temperature recuperator. Ishiyama et al. [5] presented a double recuperator, double compressor layout where heat coming from the divertor is used after the low-temperature recuperator and power from the blanket, after the high-temperature recuperator. Additionally, tritium is more straightforward to recover from S-CO_2 than from water [5], one of the most common thermal fluids used in power plants. An S-CO_2 Brayton cycle could be an adequate solution for DEMO, as it has an excellent performance in this medium temperature range. In this text, the term power conversion system refers to the S-CO_2 cycle (this is the power block that converts thermal power into electricity), and fusion power plant comprises the whole system: reactor, auxiliary systems and power conversion system.

The most realistic and conservative DEMO design, named DEMO1, is based on a pulsed reactor that will possibly require a thermal energy storage (TES) system to ensure continuous operation [3,19]. Currently, there are three main processes used to store thermal energy. The sensible heat storage (SHS) [20,21] uses the incoming thermal power to increase the temperature of the storage material during loading periods. During the unload process, the material cools down. Phase-change materials (PCM), also known as latent heat storage, store the energy as the phase-change enthalpy of the storage material [22–24]. Thermochemical energy storage (TCES) is based on reversive, endothermic/exothermic reactions, that store/release energy in the chemical bonds of the reactants [25–27]. These technologies are evaluated as possible solutions for a DEMO1-like reactor TES system.

While S-CO_2 cycles are among the most promising technologies [3] for application to fusion power plants, the power block design and integration for future nuclear fusion reactors is still an open issue. The study of optimised systems integration based on reactor characteristics and power block performance are required. There are outstanding questions regarding their integration with current reactor designs and their operation, and potential advancements in materials and achievable temperatures. Along this line, this paper analyses the integration of different variations of the S-CO_2 cycle with a DEMO-like fusion reactor. These variations are defined to incorporate the different heat sources

foreseen for DEMO at different temperature levels. The methodology is based on the definition of a framework integrating the system code PROCESS [28,29] for reactor evaluation and the numerical solver EES [30] for power blocks. PROCESS is a system code developed by the Culham Centre for Fusion Energy (CCFE) to model a fusion power plant. This framework has been used to assess the thermodynamic and economic performance of the proposed cycles.

This paper is structured as follows. Section 2 introduces the boundary conditions regarding available heat sources and the DEMO reactor and breeding blanket topology. Section 3 analyses the TES and assesses their suitability for a fusion power plant. Section 4 presents the pulsed and steady-state layouts to be analysed. In section 5, the performance of the layouts is compared in terms of their cycle efficiency and Levelized Cost Of Electricity (LCOE). Finally, the main conclusions of this work and outlook are presented.

2. Heat sources in a DEMO-like reactor

Two options are currently being considered for the design and operation of a DEMO reactor: DEMO1 [31] and DEMO2 [19,32,33]. DEMO1 is a pulsed reactor, in which the operation of the reactor is discontinuous, following the current tokamak [34] reactor designs. DEMO2 is based on a steady-state design, considering advances in reactor technology able to maintain continuous operation. The former is based on a more conservative approach, where technical and physics advancements cannot support the steady-state imposed in DEMO2.

Fig. 1 shows the available heat sources in the DEMO reactor design. The first wall is the first material layer exposed to the plasma. The breeding blanket is the primary heat source for a DEMO-like reactor. Here, the tritium required in the fusion process is bred. The divertor collects helium "ash" and other impurities (such as eroded particles from the tokamak walls) coming from the plasma. The shield constitutes a protective layer that stops particles from escaping. In 2005, the European Fusion Development Agreement (EFDA) proposed four cooling scenarios for the blanket, starting from a fundamental and technically ready approach to more advanced and optimistic systems [35,36]:

Model A: Water-cooled lithium-lead. The cooling of the breeding blanket is carried out by water, while the tritium breeding by lithium-lead. The temperature is limited by water evaporation. An upgraded version, model AB or HCLL (helium-cooled lithium-lead), changes water with helium. The usage of helium allows for higher temperatures. For both cases, the divertor and the shield are water-cooled.

Model B: Helium-cooled pebble bed (HCPB). Pebbles of beryllium are embedded in the lithium. The cooling scheme is the same as in model AB.

Model C: Dual coolant blanket. Lithium-lead breeds tritium and cools the blanket together with helium. Higher temperatures are reached due to technological advances.

Model D: Self-cooled blanket. Lithium-lead is used for tritium breeding and cooling. Temperatures around 1100ºC are expected [37].

Currently, WCLL and HCPB have been chosen as the best options, as they are the most realistic and practical approaches [38,39]. These model structures are designed to be constructed using EUROFER97, a low-activation martensitic steel that can withstand temperatures up to 550ºC [40]. HCPB will be used as the reference breeding blanket in this work.

The DEMO Baseline 2018 [31,38] is the latest official DEMO design. It contains the main physics and engineering parameters that define the DEMO1 reactor. The DEMO Baseline 2018 has been obtained by minimising the major radius of the tokamak through the system code PROCESS. The data from this baseline is used in this work to simulate a set of S-CO_2 Brayton cycles. The main heat sources are categorised as the blanket and first wall (BNK), divertor (DIV) and shield (SHD). BNK provides most of the power with 2.2 GWt of the 2.6 GWt total. The BNK temperature is limited to 550ºC because of using EUROFER97 steel due to its adequate performance under neutron bombardment. This steel usage sets a maximum temperature of 500ºC on the coolant side to account for a safety margin with EUROFER97 and thermal losses in the heat exchange process. In this baseline, DIV and SHD are expected to be water-cooled, which sets a maximum temperature of 150ºC to avoid the phase change of the coolant. The heat sources specifications are shown in Table 1.

The power requirements for the reactor and auxiliary systems are specified in the DEMO Baseline 2018. These contain the power needed to start and maintain the plasma, the tritium treatment plant, the cryoplant for the high-temperature superconductors used for the coils, poloidal and toroidal coils and helium and water pumps. The total required power is 491.9 MWe, with the primary coolant pumps consuming approximately half of it. A breakdown of these consumptions can be found in Table 2. The present study does not consider an increase in the heating and current drive consumption for the DEMO2 scenario compared to the DEMO1 scenario. In contrast, previous studies indicate this consumption could significantly increase to sustain a steady-state scenario [41].

To summarise, the DEMO Baseline 2018 proposes an HCPB breeding blanket with a EUROFER97 structure that limits its temperature to 500ºC. The DIV and SHD are water-cooled, so the water temperature cannot exceed 150ºC.

3. Thermal energy storage for fusion power plants

The DEMO1 concept follows a pulsed reactor design. This arises a set of problems related to the working lifetime of the turbomachinery and the efficient operation of the power conversion system. A cycling operation would induce thermomechanical fatigue on the turbine and other components of the power cycle, reducing their expected lifetime drastically. It implies that the pulsing operation mode of the reactor will generate partial load operation in the power cycle during a relevant part of the time, with successive loading and unloading ramps. Under these operating conditions, far from the rated conditions, the power conversion system efficiency will be penalised. Thermal energy storage (TES) is an effective way of facing these issues, as it will provide thermal power whenever the reactor is not available [3,19]. During the pulse, a fraction of the power generated by the reactor will be used to charge the TES,

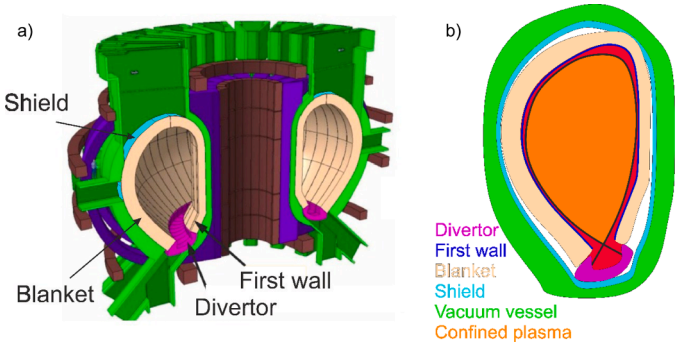

Fig. 1. a) DEMO schematics with the available heat sources. Reprinted from Fusion Engineering and Design, Vol. 109, T. R. Barret et al., Progress in the engineering design and assessment of the European DEMO first wall and divertor plasma facing components, page 8, 2016, with permission from Elsevier. b) DEMO cross-section schematic.

Table 1
Heat source specifications from DEMO Baseline 2018 following a breeding blanket model B.

Heat Source	T_{max} [ºC]	Power [MWt]	Coolant
BNK	500	2254.0	Helium
DIV	150	389.5	Water
SHD	150	1.5	Water

Table 2
Electric power needs in the DEMO Baseline 2018 as obtained from the PROCESS code.

Heating and current drive	127.5 MWe	Primary coolant pumps	234.0 MWe
Vacuum pumps	0.5 MWe	Tritium plant	15 MWe
Cryoplant	39.9 MWe	Toroidal field coils	9.5 MWe
Poloidal field coils	0.6 MWe	Other	64.8 MWe

which will unload during dwell time. Harrington et al. [42] proposes a water-cooled DEMO1 Rankine cycle with no energy storage system. This study concludes that the turbine would not show significant thermal-induced stress if kept spinning during the dwell time. This study also points out that avoiding a TES in a He-cooled reactor would be inherently more challenging due to a more significant pumping consumption and more substantial inlet/outlet temperature differences.

Different papers on pulsed nuclear fusion reactors acknowledge the importance of adding a TES system. Lucas et al. [43] reviews several energy storage systems and argues that only hydrogen and TES systems can scale to the needed sizes. Amongst the TES options, molten salts (a PCM material) are the most promising ones for this application. The same conclusion has been reached by Kovari et al. [3]. [44] introduces a TES system based on the usage of solar salts.

Table 3 shows a comparison of relevant parameters for the TES systems. This table depicts the normal range of actuation of these technologies, but there are specific cases where some materials may be outside these limits. For example, cast steel (an SHS material) has a storage capacity of 450 kWht/m^3, a heat conductivity of 40 W/mK and an estimated cost of 60 $/kWht.

As the DEMO Baseline 2018 is modelled based on a DEMO1 scenario, a TES is required to ensure continuous operation and to avoid partial load and material fatigue that could be disastrous for high inertia elements, such as the turbines. In this baseline, the DEMO pulses last 2 hours with a dwell time of 30 minutes, the ramping between both stages requires 10 minutes. A TES system for a DEMO-like fusion power plant will have the following requirements:

The working temperature is in the range of 500ºC for the BNK power source and 150ºC for the DIV and SHD.

It must have a good heat transfer capacity. The unloading cycle must be completed in 30 minutes. Therefore, high conductivity is highly recommended to avoid an oversized and underused TES.

It must have an extended lifetime. The TES will be subject to constant cycling within the fusion power plant lifetime.

Safety and stability. The TES is framed in a nuclear facility. Therefore, the used material must be chemically stable and present low safety risks. The storage material must be able to withstand radiation, as it is expected to get to the TES through the reactor coolant.

Tritium recovery. Some tritium from the breeding blanket will inevitably reach the TES system. The storage material must not interact with it, and it must be easy to separate from the tritium for its recovery.

The first point is easily achievable for all studied technologies, as shown in Table 3, but the significant temperature difference of the thermal sources indicates the utilisation of two TES systems [48]. The best option in terms of heat transfer capacity is based on SHS materials. The TCES heat conductivity is not shown as it heavily depends on the kinetics of the thermo-chemical reaction and the state of the products. To date, the safety design concerns suggest the utilisation of well-known and mature technologies, and currently, this is an advantage of SHS and PCM over TCES. However, relevant advances have been achieved in the last years in TCES, with advantages regarding the required storage volume. The stability under radiation and the need for tritium recovery require further analysis.

Using molten salts would suppose an isothermal heat exchange process and less volume, but significant advances must be made to reach the technical maturity level expected for this task. Two different molten salts with different melting temperatures can be used: one for the high-temperature source (BNK) and another for the low-temperature sources (DIV and SHD). On the other hand, solar salt is an SHS well-known material commonly used for concentrated solar power plants with a maximum working temperature of 621ºC [21]. Solar salts can be used for the BNK, while water could be used for DIV and SHD, as using the same material for heat transfer and storage ensures the best possible coupling. Table 4 shows a comparison between both options, molten salts (PCM) and solar salt and water (SHS). A 200 K difference between the cold and hot tanks is considered [49]. The cost of molten salts takes into account the existence of two different temperature heat sources [43]. The SHS option is significantly cheaper, but PCM technologies are still under development, so there is still room for lower costs for this option.

4. Methodology. Integration with power cycles

For the analysis of the integration of different power cycles configurations with the fusion reactor, a framework integrating the system code PROCESS [28,29] for reactor evaluation and the numerical solver EES [30] for power block performance was defined. It allows the assessment of the thermodynamic and economic performance of the proposed integrations.

PROCESS is a system code developed by the Culham Centre for Fusion Energy (CCFE) to model a fusion power plant. This code comprises a set of physics and engineering modules that solve optimisation problems for the complete fusion power plant. The framework developed here uses the boundary conditions and the power availability obtained with the PROCESS code to evaluate the power cycle in EES. The results from these power cycle simulations are used as inputs in the PROCESS code to assess the total plant costs. From these, the LCOE is calculated.

The data obtained from the DEMO Baseline 2018 is used to simulate a set of S-CO_2 Brayton cycles with different configurations to identify their fit to the available heat sources. A total of fourteen layouts, twelve for DEMO1 and two for DEMO2, are studied. Recuperators are used to take advantage of the high temperature at the turbine outlet. The pressure drop in heat exchangers has been set to 0.4 bar and the minimum temperature difference to 4.5ºC for the Low-Temperature Recuperator (LTR), 4ºC for the High-Temperature Recuperator (HTR) and 4ºC for single recuperator cases. During reactor operation (DEMO1 pulse time and DEMO2 complete operation), the efficiency at rated conditions has been fixed at 88% for compressors and 93% for the turbine. These efficiencies drop at partial loads to 85% and 91% respectively during dwell time for DEMO1 [50,51]. The generator efficiency is fixed at 97% [17].

A review of structural materials compatible with a fusion reactor has

Table 3
Comparison of the main parameters of the available TES technologies [22, 45–47]

	Storage capacity [kWht/m^3]	Heat conductivity [W/mK]	Temperature [ºC]	Cost [$/kWht]
SHS	52 – 160	0.1 – 7	300 – 700	1 – 7
PCM	43 – 297	0.5 – 2	110 – 900	1 – 5
TCES	720 – 1220	n.a.	200 – 2300	12 – 50

Table 4
Economic assessment for a molten salt and a combined solar salt and water TES systems [22,43,49]

Molten salts (PCM)		Solar salt and water (SHS)	
Cost [$/kWh]	24.58	Cost solar salt [$/kWh]	20
Energy [MWh]	1058	Energy BNK [MWh]	901.6
		Cost water [$/kWh]	0.0113
		Energy DIV+SHD [MWh]	156.4
TOTAL	**26.00 M$**	**TOTAL**	**18.03 M$**

been performed to determine the maximum operating temperature for designs beyond the reference DEMO1 baseline. Structural materials in fusion reactors are affected by neutron irradiation and high fluxes of heat and particles that may damage them. The neutron flux produces hundreds of dpa (displacements per atom) in the structural materials [52]. Materials in fusion environments are also affected by significant levels of transmutant H/He that can embrittle the structure. Low activation materials must be pursued to reduce the radiation damage and to mitigate the disposal issues after the lifetime of the reactor [53].

Zinkle et al. [54], studies the upper operating temperature of a series of candidates. Being some of the most remarkable ones the reduced-activation ferritic/martensitic steels (RAFM), that can withstand up to 550ºC and forms the current choice for the DEMO Baseline 2018; the Oxide Dispersion Steel (ODS) [55], ~750ºC of maximum operating temperature and the SiC/SiC composites [56], that can achieve up to 1000ºC. This brief review can conclude that a higher temperature can be achieved in a more optimistic/advanced DEMO scenario where new structural materials are developed up to the industry standards.

The recuperator in S-CO_2 cycles can present challenges regarding its thermal integration. These challenges are linked to the feasible minimum temperature difference between streams (pinch point) that, due to carbon dioxide behaviour, can occur inside the heat exchanger [7]. The low-pressure side of this recuperator can come close enough to the critical point that its properties vary significantly with respect to the high-pressure side. As shown in Fig. 2, the variation of heat capacity (C) leads to the minimum temperature difference being inside the recuperator and not at its inlet or outlet, as commonly expected. This is typically solved by ensuring enough temperature difference at the heat exchanger inlets. The minimum temperature difference (TD) in the heat exchanger is found at the point where the heat capacity is equal on both sides (Fig. 2). Despite this, a heat exchanger working with S-CO_2 close to the critical point can still be balanced by reducing the mass flow of the hot stream. This is achieved by bypassing a fraction of the hot stream mass flow to the low-temperature recuperator. In recuperators with higher temperatures, as the c_p does behave normally, the total mass flow can be introduced at both sides. In this work, the bypass fraction is used as an optimisation variable to obtain the maximum power block system efficiency, while always ensuring that the cold stream temperature never surpasses the hot stream inside the heat exchanger. Table 6 shows the mass fraction (α) for the different layouts, for most cases it is found to be ~0.3. Linares et al. [57] is in agreement with this α value in a study of a different S-CO_2 power block system for a DEMO-like reactor. It is important to note that different layouts will have different optimisation points for this variable and they should be address individually.

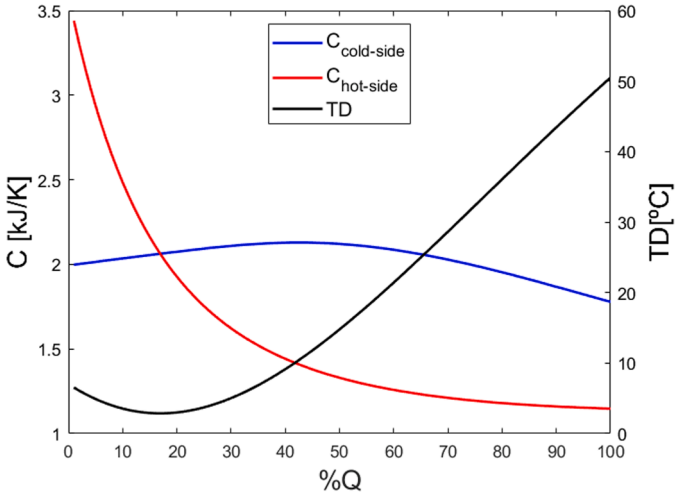

Fig. 2. Representation of the pinch-point evolution in a S-CO_2 heat exchanger.

The EES numerical solver software was used for modelling the power cycle, the layout designs and optimisation [9]. Carbon dioxide properties were evaluated from the equation of state proposed by Span and Wagner [58], valid up to 1100 K and 800 MPa. All simulations were below these limits.

Fig. 3 shows the integration framework developed in this work between the PROCESS code and EES to assess the thermal and economic parameters of the cycle layouts. First, the DEMO Baseline 2018 is obtained from the PROCESS code. The cycle layouts are modelled in the EES software, taking into account the heat sources parameters and reactor and auxiliary consumptions from the DEMO Baseline 2018. The net electric efficiency of the complete fusion power plant ($\eta_{elec,plant}$) is optimised for these layouts. The optimisation variables will be the inlet parameters (temperature and pressure) for the compressor and turbine and the mass fraction flowing through the secondary compressor (α). The resulting plant efficiency and net electricity production (W^{net}_{elec}) are then introduced in the PROCESS code together with the economic parameters from the DEMO Baseline 2018 to carry out an economic assessment of the cycle. The total cost of the fusion power plant is obtained from this economic assessment and the LCOE of the different layouts is calculated.

One of the most notable differences between DEMO1 and DEMO2 regarding cycle integration is the operation mode: pulsed in DEMO1 and steady-state in DEMO2. Therefore, the integration has been divided into two subsections, one for each scenario.

4.1. Pulsed layouts

The pulsed layouts are modelled based on the DEMO1 design. A pulsed reactor is the most plausible and conservative option for a future DEMO-like fusion power plant, as it requires the least physics and engineering advancements from the current tokamak designs [41]. A thermal energy storage system must be included to avoid cycle fatigue on the power conversion system components that could severely decrease its expected life. The TES system will load up during the pulse time and release the stored thermal energy during the dwell time. It has been modelled as a black box where energy fed is stored during the pulse time to give it back to the cycle during the dwell time. A thermal-to-thermal efficiency (η_{TES}) of 95% has been chosen to account for the heat losses as a percentage of the stored energy [59]. The TES system integration in the layout is shown in Fig. 4. The electric efficiency of a DEMO1-like power conversion system (η_{pcs}) has been defined in terms of its energy production over a complete operation cycle, as shown in equation 1.

$$\eta_{pcs} = \frac{W_{elec}}{Q_{DEMO}} = \frac{\dot{W}_{pulse} * t_{pulse} + \dot{W}_{dwell} * t_{dwell} + \dot{W}_{ramp} * 2 * t_{ramp}}{Q_{DEMO}} \quad (1)$$

Here, W_{elec} is the net electric energy produced in a complete DEMO1 cycle (defined as $t_{cycle} = t_{pulse} + t_{dwell} + 2 * t_{ramp}$). Q_{DEMO} is the energy delivered by DEMO1 during a cycle. $\dot{W}_{pulse}$, $\dot{W}_{dwell}$ and $\dot{W}_{ramp}$ correspond to the power produced during the pulse time (t_{pulse}), dwell time (t_{dwell}) and ramp time (t_{ramp}). For the ramp time, the generated power is supposed to be the average between the pulse and dwell power.

The thermal power received by the TES system and by the cycle varies during the pulse and dwell time. Eqs. (2)-(4) show the thermal power distribution during the different periods:

$$\dot{Q}_x = \dot{Q}_x^{TES,\ pulse} + \dot{Q}_x^{pcs,pulse} \quad (2)$$

$$Q_x^{(TES,pulse)=(Q_x)} * \frac{(t_{dwell} + 2 * t_{ramp})}{t_{cycle}}; \quad (3)$$

$$Q_x^{(pcs,pulse)=(Q_x)?} * \frac{t_{pulse}}{t_{cycle}}$$

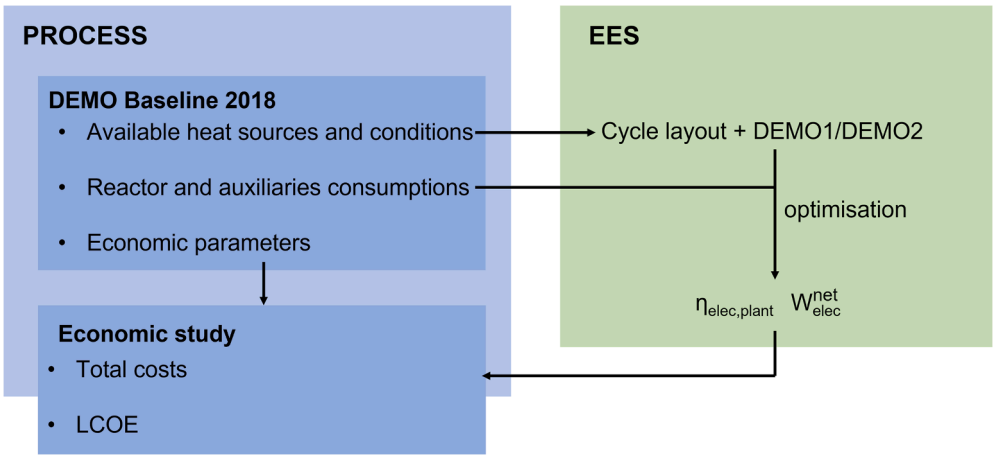

Fig. 3. Integration of the PROCESS code and EES to assess the optimum efficiency of a cycle layout and its related costs.

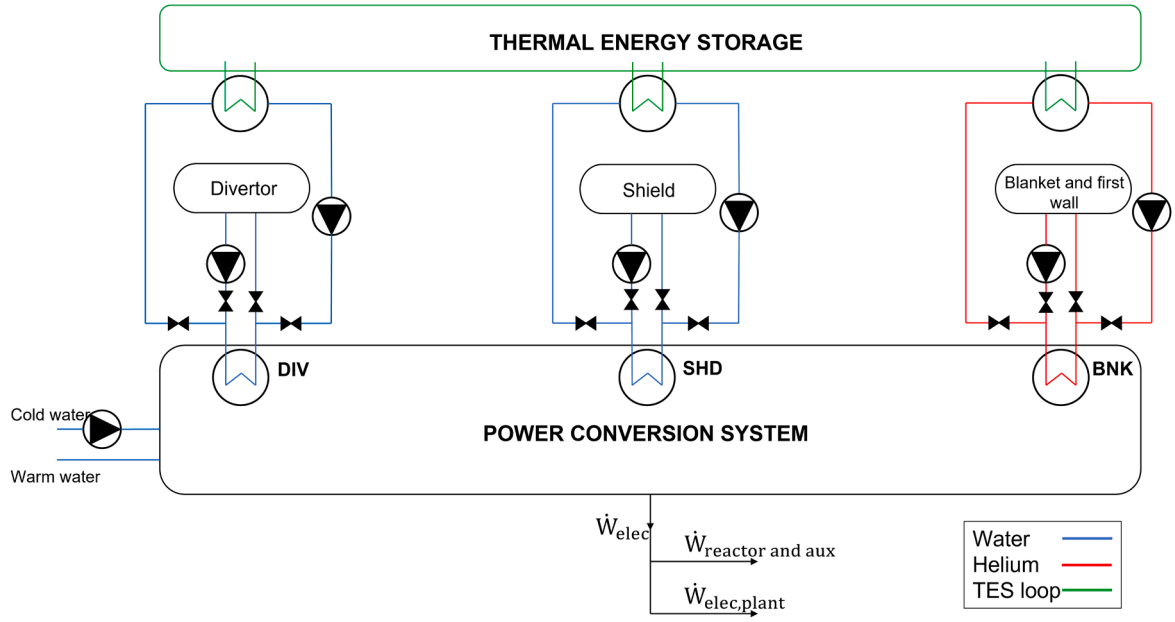

Fig. 4. Thermal energy storage integration in the fusion power plant layout. The loops external to the power cycle are presented: cooling water (blue), helium (red) and TES loop (green) (For interpretation of the references to color in this figure legend, the reader is referred to the web version of this article).

$$\dot{Q}_x^{TES\rightarrow pcs} = \frac{Q_x^{TES,pulse}}{t_{dwell} + 2 * t_{ramp}} * \eta_{TES} \quad (4)$$

where x = BNK, DIV or SHD. $\dot{Q}_x$ is the heat power provided for the aforementioned heat sources during the pulse time, this is divided between the TES ($\dot{Q}_x^{TES,pulse}$) and the power conversion system ($\dot{Q}_x^{pcs,pulse}$). The stored energy (Q^{TES}) is fed into the power conversion system ($\dot{Q}^{TES\rightarrow pcs}$) during the dwell and ramp times.

The DEMO heat sources in the pulsed state present several temperature limitations. The DIV and SHD, are water-cooled with a maximum temperature of 150ºC. BNK uses the ferritic/martensitic steel EUROFER97 as a structural material, stable under neutron bombardment, but with a maximum temperature of 500ºC. In order to study the optimal integration of the heat sources and the impact of the positioning of the cycle elements on the cycle performance, three variations are proposed for the low-pressure side of the cycle and another three for the high-pressure side, adding up to a total of nine combinations. Three more variants are presented based on more advanced versions of DEMO1. All of them follow the schematic shown in Fig. 4.

The low-pressure side variations are related to the positioning of the HTR, LTR, and secondary compressor. They are: HLC (HTR-LTR-secondary compressor), HCL (HTR-secondary compressor-LTR) and NC (No secondary compressor). In HLC layouts, the LTR presents a higher mass flow in the low-pressure side as part of the total mass flow will bypass it in the high-pressure side. This configuration means that the temperature evolution in the LTR can be modified directly by the mass fraction flowing through the secondary compressor (α). The HCL layout features a mass-balanced LTR. The NC layouts suppress the secondary compressor to determine whether the extra consumption of the compressor is worth it in terms of the overall electric efficiency.

High-pressure variations rely on the relative position of the shield, divertor and LTR. The high-pressure variations aim to discern the best positioning for the heat sources due to their temperature constraints. The naming convention used is DSL (divertor-shield-LTR), LDS (LTR-divertor-shield) and NDS (no divertor and shield). The DSL layout places the low-temperature heat sources first to avoid losing part of their power due to exceeding the temperature limit. This issue could arise in the LDS case, where the LTR is at the main compressor outlet and its high-pressure side outlet is constrained by the temperature limit of the DIV

and SHD. As an advantage of the LDS layout, the LTR can go to a lower temperature at its low-pressure outlet. It means that less power is dissipated in the cooler. The NDS layouts do not include the DIV and SHD to operate at higher temperatures, avoiding the operational constraint linked to their temperature thresholds. It disregards the usage of the heat available in these components.

Layouts HCL.LDS-HT1, 2 and 3 are upgraded versions of layout HLC.LDS. They follow the same scheme, but a DEMO1-like reactor with technical advancements is assumed to account for potential future structural materials and engineering developments. In Section 4, the upper-temperature limit set by the current under-research structural material was discussed. A SiC/SiC structure is expected to withstand temperatures up to ~1000ºC under reactor-like radiation [54], but further research is necessary to become a mature material integrated under the operational conditions. Type HLC.LDS-HT layouts feature a temperature limit of 800ºC set by the usage of an S-CO_2 cycle. At this 800ºC limit, S-CO_2 cycles are in the range known for showing clear advantages over ordinary gas turbines [9,60]. For this new advanced scenario, the maximum achievable temperature in the BNK has been set at 800ºC. The DIV and SHD are now helium-cooled, so they will also get to 800ºC. To operate at higher temperatures an ordinary Brayton cycle is recommended, which is not in the scope of this paper. The influence of varying the maximum cycle temperature for all layouts is studied in section 5. The three HLC.LDS-HT layouts present the same limits in terms of temperatures and pressures, but different dwell and pulse times are set for each case to study the influence of these parameters on the efficiency of the system. Layout HLC.LDS-HT will follow the DEMO Baseline 2018. This is 2 hours long pulses with 30 minutes of dwell time; on the other hand, HLC.LDS-HT1/HLC.LDS-HT2 feature 4/6 hours pulses and 20/10 minutes dwell time.

HLC.LDS-HT1 is intended as a more optimistic scenario from the technological point of view, with advances in materials and/or systems integration. However, it is still conservative in the physics assumptions (i.e., the operation of a DEMO2-reactor is still not achievable, and the reactor operates in pulses). HLC.LDS-HT2 and 3 increase the pulse duration in order to study the repercussion of pushing this limit. The work presented in this paper is based on the DEMO Baseline 2018, the latest official version. Note that these HLC.LDS-HT DEMO designs are intended as bridge scenarios between the realistic pulsed DEMO1 and the optimistic steady-state DEMO2. Other combinations of parameters (i.e., advancements in the physics understanding, but not in the technical aspects) could find their place in this intermediate scenario.

The twelve resulting combinations are summarised in Table 7. A single recuperator will be used for cases where LTR and HTR would be directly connected in both the hot and cold sides (layouts NC.DSL and NC.NDS).

Changing the LTR positioning at the low-pressure side implies that the mass flows on both sides of the recuperator can be equal (HCL and NC scenarios) or with a lower mass flow in the cold side of the heat exchanger (HLC scenario). In the HLC scenario, α will directly affect the outlet temperature of the cold side of the LTR. The NC layouts explore whether adding an extra component to the cycle, with its corresponding power consumption, is profitable or not.

The combinations related to the high-pressure side study the impact of the maximum temperature, 150ºC, set at the divertor and shield by the DEMO Baseline 2018. DSL avoids this constrain by heating the mass flow at its coldest high-pressure point, where the provided power by both heat sources is not large enough to heat the mass flow over 150ºC. LDS checks the importance of this restriction, as it directly limits the heat exchanged in the LTR to not overcome the temperature limit. NDS directly excludes these heat sources from the layout.

4.2. Steady-state layouts

The steady-state layouts will be based on a DEMO2-like fusion reactor. In this scenario, the plasma pulses are assumed to be continuous. The boundary conditions imposed for these layouts have been relaxed as DEMO2 requires relevant technical improvements. The temperature limits are the same as in layout HLC.LDS-HT (section 4.1). DIV and SHD will be helium-cooled, letting the outlet temperature overcome the 150ºC barrier imposed by the previous water-cooled system. Upgrades on the structural materials can also be expected in the following decades. Therefore, the temperature limit imposed by the EUROFER97 is removed, and the maximum achievable temperature is set from 500ºC to 800ºC. The S-CO_2 Brayton cycle may not be the optimal choice for higher temperatures, and other gas turbine technologies can have better performance and fewer integration challenges depending on the temperature range. The rest of the parameters have been taken from the DEMO Baseline 2018 and correspond to the pulsed state simulations.

Two steady-state layouts have been modelled based on the HLC.LDS layout (Fig. 5), the most efficient cycle between those studied for DEMO1. A summary of the main parameters of the layouts is shown in Table 6 and Table 7. The prefix “SS” is added to indicate the layout is in steady-state. SS-HLC.LDS (Fig. 6 a)) is a direct copy of HLC.LDS but with no TES and the softer constraints expected for DEMO2. SS-HLC.LDS-2T (Fig. 6 b)) features a second turbine with an intermediate reheater. The BNK power will be split between two heat exchangers to heat the fluid right before passing through each turbine.

4.3. Parameter range for the proposed layouts

Table 5 represents the studied range of the optimisation variables used in the optimisation process in EES. There are three types of reactor models to study: DEMO1, a pulsed reactor; DEMO1-HLC.LDS-HT, a pulsed reactor with more technical advancements and DEMO2, a steady-state reactor. The inlet temperature to the compressor is not included as it has been introduced as a function of the inlet pressure. For an inlet pressure greater than 80 bar, the inlet temperature will be 30ºC. This temperature will linearly increase to 36ºC at 75 bar to leave a safety margin of 5ºC with the carbon dioxide critical point. This will penalise the cycle efficiency but will ensure not passing the critical point. α has been limited to 35% of the total mass flow as for higher values the cycle efficiency decreases rapidly, as shown in section 5. The turbine inlet pressure has been capped at 280 bar to comply with the S-CO_2 technology standard [17]. As stated in section 2, the turbine inlet temperature limit is set by the usage of EUROFER97 and the thermal losses associated with the primary coolant system.

5. Results

5.1. Comparison of the different layouts

A sensitivity analysis has been carried out to determine which parameters are the most significant for the cycle. The figure of merit is the electric efficiency of the power cycle. The studied parameters are the inlet temperature and pressure at the turbine, the inlet pressure at the compressor and the mass fraction flowing through the secondary compressor (for cases different to the NC layouts).

Table 6 presents the optimised cycle parameters given by the optimisation process followed through this section. These values result in the efficiency and electric production shown in Table 7. Two versions of the SS-HLC.LDS-2T cycle with different maximum temperatures are included: an 800ºC turbine inlet temperature cycle (optimum temperature) and a 500ºC turbine inlet temperature cycle. This lower temperature version is intended as a bridge scenario where physics advances would allow the usage of a steady-state fusion reactor, but structural materials cannot surpass the 500ºC barrier.

The LDS combinations are the optimal layouts for every low-pressure variation, as shown in Table 7. The temperature limitation set by the DIV and SHD did not penalise the overall efficiency as much as it could be expected. The extra power added to the system by the DIV and SHD

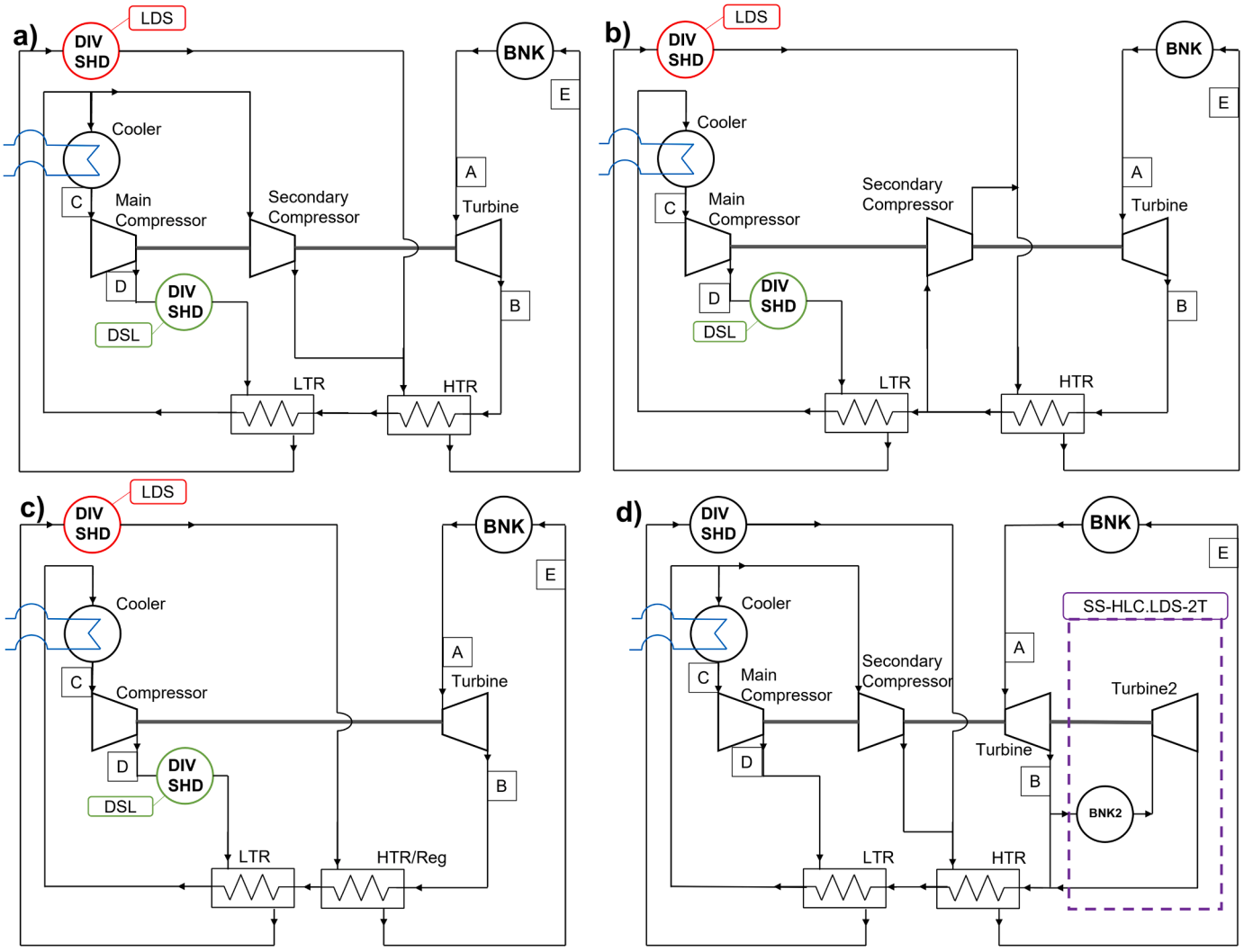

Fig. 5. Schematic of presented layouts. a) Layouts type HLC, b) type HCL, c) NC, d) type SS-HLC. Coloured parts of the layout represent the parts that belong exclusively to the noted layouts. The blue colour represents cooling water (For interpretation of the references to color in this figure legend, the reader is referred to the web version of this article).

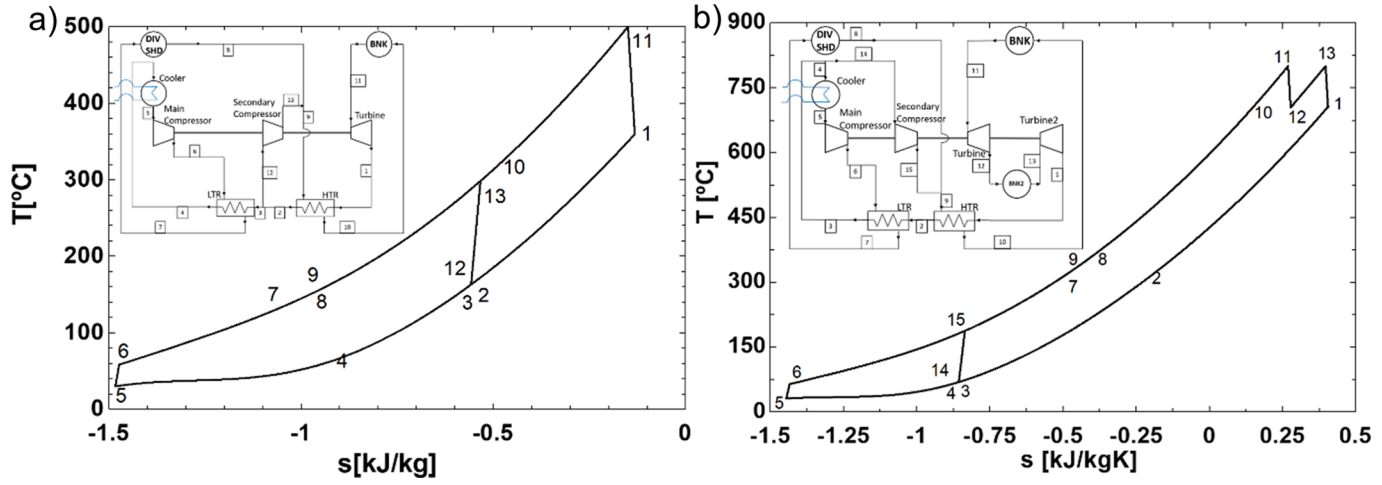

Fig. 6. Temperature - entropy diagram for the a) HCL.LDS (DEMO1) and b) SS-HLC.LDS-2T (DEMO2) cycles. Both using the maximum allowable temperture compatible with their structural materials.

Table 5
Parameter range of the optimisation variables.

Parameter	DEMO1	DEMO1-HLC.LDS-HT and DEMO2
$T_{turbine}$ [°C]	350 – 500	500 – 800
$p_{turbine}$ [bar]	200 – 280	200 – 280
$p_{compressor}$ [bar]	75 – 85	75 – 85
α [-]	0 – 0.35	0 – 0.35

surpass the efficiency penalty induced by the temperature limit (that also produces a limit on the α). The NDS layouts have a lower electric efficiency than their counterpart. The basis of this design, to avoid the temperature limitation imposed by DIV and SHD, does not compensate for the heat not used from these components (391 MWt).

The LDS type layouts show better results than their equivalent DSL, thanks to the capability of the LTR of working at lower temperatures. In the DSL layouts, the high-pressure stream is first heat up by the divertor and shield before entering the LTR and, therefore, the hot stream will not be as cooled as in the LDS cycles. Thus, more energy will be used in the LDS than in the DSL cases and the efficiency of the former will be improved.

A series of simulations have been carried out without the TES system to study its impact. The analysed systems are the HLC.LDS, HCL.LDS and NC.LDS showing efficiencies on the power block system of 42.97, 42.11 and 41.62%, respectively. This is approximately a 4% increase from the TES scenario. The period where the TES feeds the cycle is not at rated conditions penalising the overall efficiency. The TES protects the secondary loop from thermo-mechanical cycling at the cost of power production. Future work must be carried out to determine the effect on the turbomachinery of not including TES.

In Table 7, m is the mass flow through the turbine; W^{net}_{elec}, is the net electric output of the power plant, η_{pbs} is the power block system efficiency (Eq. 1) and $\eta_{elec,plant}$ is the power plant electric efficiency (Eq. 5) [57]:

$$\eta_{elec,plant} = \frac{W_{elec} - \dot{W}_{power\ needs} * t_{pulse}}{Q_{DEMO}} = \frac{W^{net}_{elec}}{Q_{DEMO}} \quad (5)$$

where $\dot{W}_{power\ needs}$ are the electric power consumptions shown in Table 2.

Steady-state simulations show a significant increase in the electric efficiency of around 20% due to the constant operation and less restrictive temperature conditions. As already stated, SS-HLC.LDS is a direct conversion of the HLC.LDS layout into the steady-state version as this layout achieved the best results of the pulsed layouts in terms of efficiencies. The second turbine added in SS-HLC.LDS-2T contributes to a 1.4% improvement in the electric efficiency of the cycle and additional power of 35.7 MWe.

Fig. 7 shows the turbine inlet temperature dependence of the LDS layouts. These will be the represented layouts at the sensitivity analysis as they are the most promising in terms of efficiency. Fig. 7 a) also shows the temperature dependence of the heat recovered fraction (HRF). The HRF is the fraction of the turbine outlet power that is reintroduced in the cycle in HTR and LTR (Eq. 6). Here, Q_{LTR}, Q_{HTR} and Q_{cooler} are the thermal power exchanged in the LTR, HTR and cooler, respectively. The HRF is a metric of the efficiency of the heat recovery at the low-pressure side. The denominator is the heat power available in the low-pressure side and the numerator, the heat recovered in both recuperators. For the layout SS-HLC.LDS-2T (Fig. 7), the inlet temperature of both turbines is the same as it returns the highest efficiency. This figure shows a strong dependence of the efficiency on the temperature, but this dependency slowly decreases as the temperature increases.

$$\text{Heat recovered fraction (HRF)} = \frac{Q_{LTR} + Q_{HTR}}{Q_{LTR} + Q_{HTR} + Q_{cooler}} \quad (6)$$

S-CO_2 cycles take advantage of the high temperature at the turbine outlet to boost its efficiency through recuperators. However, this requires a high temperature at the turbine inlet (as shown in Fig. 7). If this cannot be achieved, a high pressure must be imposed at the turbine inlet

Table 7
Main parameters of the analysed layouts. Here, m is the mass flow in the cycle. W_{elec} is the net power obtained in the power plant. η_{pbs} is the electric efficiency of the power block system. $\eta_{elec,plant}$ is the electric efficiency of the power plant. A low temperature version of SS-HLC.LDS-2T is included as a bridge scenario with DEMO1-like structural materials.

	Layout	m [kg/s]	W^{net}_{elec} [MWe]	η_{pbs} [-]	$\eta_{elec,plant}$ [-]
Pulsed	HLC.DSL	7372	350.2	0.374	0.188
	HLC.LDS	6756	370.6	0.384	0.199
	HLC.NDS	6994	295.6	0.344	0.158
	HCL.DSL	5675	287.9	0.340	0.154
	HCL.LDS	6899	355.8	0.377	0.191
	HCL.NDS	6602	270.1	0.331	0.145
	NC.DSL	5675	287.9	0.340	0.154
	NC.LDS	6356	348.8	0.373	0.187
	NC.NDS	5338	197.9	0.292	0.106
	HLC.LDS-HT1	6216	652.6	0.536	0.350
	HLC.LDS-HT2	7548	807.2	0.542	0.356
	HLC.LDS-HT3	8129	876.3	0.545	0.359
Steady-state	SS-HLC.LDS	8553	958.6	0.548	0.362
	SS-HLC.LDS-2T (800°C)	8248	994.3	0.562	0.376
	SS-HLC.LDS-2T (500°C)	10525	698.4	0.450	0.264

Table 6
Optimised cycle parameters for all studied layouts. Layout SS-HLC.LDS-2T present the values for both turbines. The primary coolant temperatures have been taken from the DEMO Baseline 2018. Subindexes refer to Fig. 5. A low-temperature version of SS-HLC.LDS-2T is included as a bridge scenario with DEMO1-like structural materials.

Layout	T_A [°C]	p_A [bar]	p_B [bar]	T_C [°C]	p_C [bar]	p_D [bar]	T_E [°C]	α [-]
HLC.DSL	500	280	80.78	30.5	79.9	282.0	329.2	0.32
HLC.LDS	500	280	86.2	30.0	85.0	282.0	314.0	0.08
HLC.NDS	500	280	86.2	30.0	85.0	281.2	320.2	0.31
HCL.DSL	500	280	78.4	32.8	77.6	281.6	279.8	0.00
HCL.LDS	500	280	86.2	30.0	85.0	282.0	317.8	0.09
HCL.NDS	500	280	86.2	30.0	85.0	281.2	309.5	0.20
NC.DSL	500	280	78.4	32.8	77.6	281.6	279.8	-
NC.LDS	500	280	86.2	30.0	85.0	282.0	302.6	-
NC.NDS	500	280	78.4	32.8	77.6	280.8	266.5	-
HLC.LDS-HT1	800	280	86.2	30.0	85.0	282.0	600.3	0.27
HLC.LDS-HT2	800	280	86.2	30.0	85.0	282.0	600.3	0.27
HLC.LDS-HT3	800	280	86.2	30.0	85.0	282.0	600.3	0.27
SS-HLC.LDS	800	280	80.9	30.4	79.7	282.0	594.4	0.28
SS-HLC.LDS-2T	800/800	280/148.5	148.9/80.4	31.0	79.2	282.0	682.0/704.4	0.28
SS-HLC.LDS-2T	500/500	280/148.5	148.9/80.4	31.0	79.2	282.0	404.4/422.3	0.28

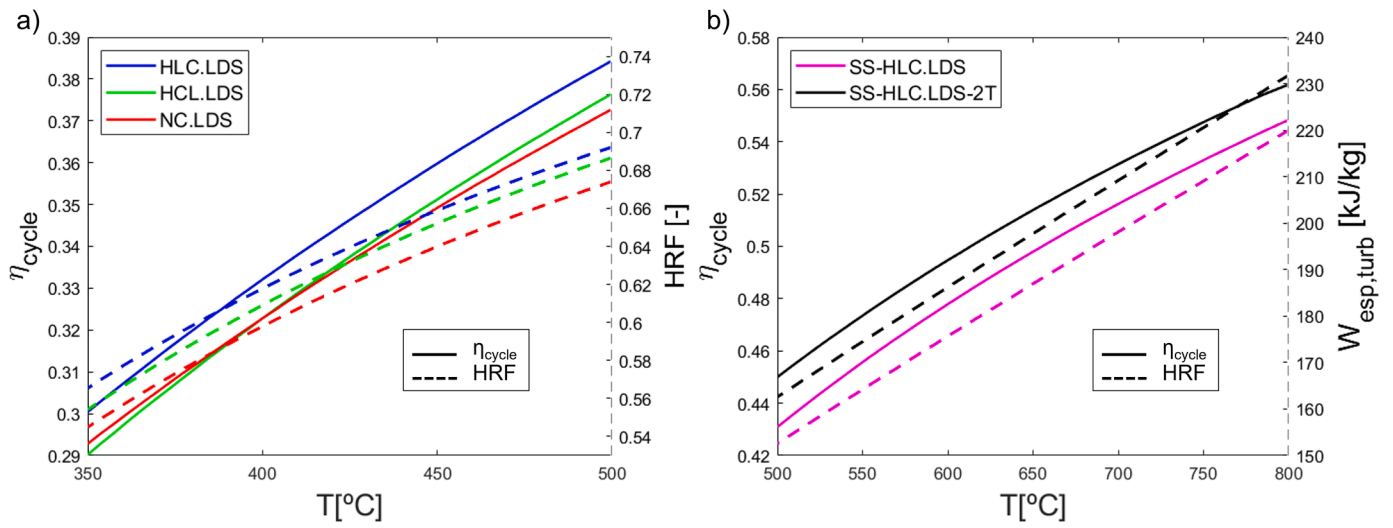

Fig. 7. a) Turbine inlet temperature sensitivity analysis for pulsed layouts of type LDS (solid line) and its HRF (dashed lines). b) Turbine inlet temperature sensitivity analysis for steady-state layouts (solid lines) and its turbine specific work (dashed lines).

to increase the outlet temperature with the corresponding extra power consumption. Therefore, a high turbine inlet temperature is mandatory in an S-CO_2 fusion power plant to exploit the heat recovery potential of the cycle and should be pursued through the search of high-temperature-resistant structural materials compatible with a fusion reactor operation.

Fig. 8 a) shows the efficiency and the HRF as a function of the turbine inlet pressure. The pressure curve follows a very similar evolution between all studied layouts. Therefore, it can be concluded that, for the given cycles, the effect of the turbine inlet pressure is independent of the chosen layout, and the maximum pressure compatible with the chosen materials and components should be pursued. However, the benefits of increasing the pressure decrease at high pressures. The equipment cost will have an important role to determine the maximum pressure of the cycle.

The influence of α on the efficiency and the power consumption of the compressors is represented in Fig. 8 b). The two steady-state layouts increase their efficiency with α, slower in the LHC.LDS case. However, this trend is abruptly ended by the DIV and SHD temperature limitation; as for larger α, the 150ºC temperature threshold is exceeded. The steady-state cases do not have this limitation and, therefore, can work in a broader range of α. The maximum efficiency occurs around 0.25-0.3, similar to those obtained in other cycles with a secondary compression [17]. If this restriction is removed the pulsed state layouts are expected to follow the same profile due to changing the coolant used for DIV and SHD. The dotted line represents the evolution of layouts HLC.LDS and HCL.LDS if the DIV and SHD temperature restriction did not exist. The Layout HLC.LDS presents a maximum at α around 0.27 as in the other cases. The efficiency of the layout HCL.LDS remains rather constant until α ~ 0.18, where it starts to decrease.

The type HLC.LDS-HT layouts are designed as bridge scenarios between DEMO1 and DEMO2. The analysis shows the importance of improving the cycle conditions that are related to the development of materials – the increase of the working temperature for the same cycle (HLC.LDS-HT1) used in HLC.LDS results in an increment in the efficiency of the plant of 15%. This increase comes from the more substantial enthalpy drop available in the turbine and a higher turbine outlet temperature to be used in the recovery subsystem. In these advanced pulsed layouts, the turbine inlet temperature is 800ºC and the mass fraction flowing through the secondary compressor is ~0.3, a parameter limited by the DIV and SHD temperature in the HLC.LDS

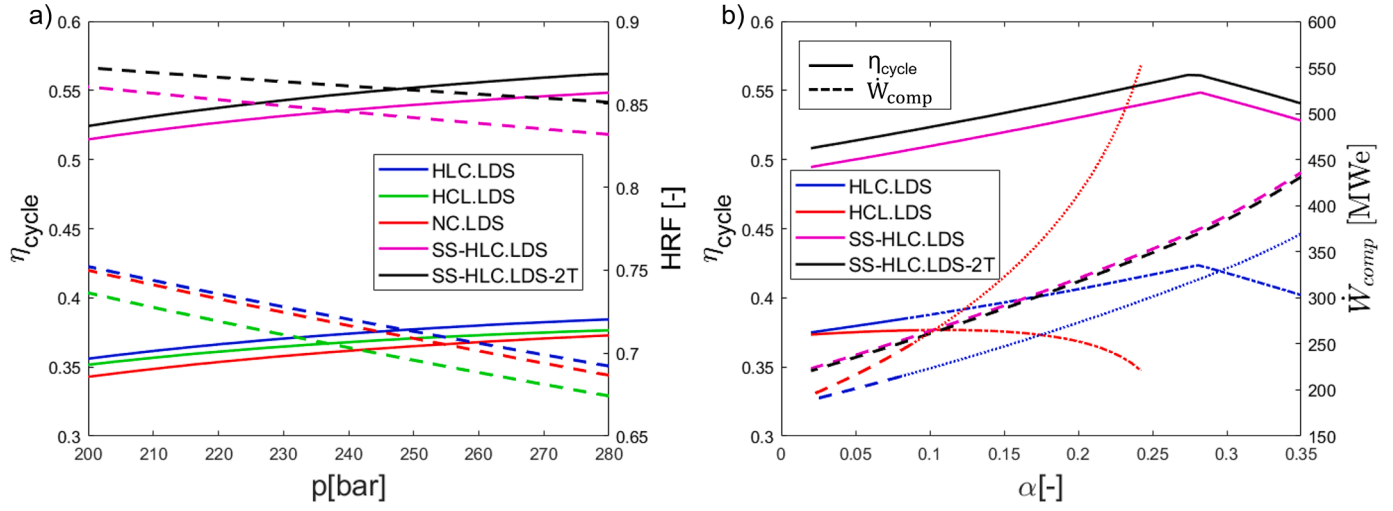

Fig. 8. a) Electric cycle efficiency (solid lines) and HRF (dashed lines) as a function of the turbine inlet pressure. b) Electric efficiency (solid lines) and compressors consumption (dashed lines) as a function of the mass fraction flowing through the secondary compressor. Dotted and dotted-dashed lines represent α values that surpass the temperature limit in DIV and SHD.

layout. HLC.LDS-HT2 and 3 show that increasing the pulse time and decreasing the dwell time can mean improving the overall efficiency of the power block system by up to ~1%. When comparing with the low-temperature DEMO1 scenarios, increasing the maximum temperature translates into better improvements than decreasing the dwell time.

5.2. Costs evaluation

This section compares the total cost and the Levelized Cost Of Electricity (LCOE) of the most efficient layouts (LDS and advanced pulsed scenarios and both steady-state cycles). The total costs include all the direct and indirect costs related to the construction of the reactor, power cycle and all the auxiliary systems necessary for operation. The total costs are estimated using the PROCESS code. The PROCESS code presents two cost models: the 1990 cost model [61] and the 2015 Kovari model [62]. The 1990 cost model has been chosen to assess the capital and indirect costs of the fusion power plant, as the 2015 Kovari model estimates only the capital costs of the plant. Due to their relatively short lifetimes, the blanket, the first wall, the divertor and a fraction of the current drive system are considered as fuel costs. These costs are related to an international first-of-a-kind fusion power plant, so it is expected that they will decrease in the successive generations of reactors, through the learning curve of technology. The PROCESS code is based on the Generomak scheme [63] and other system codes, such as the TETRA code [64]. Costs given by this code are estimated in 1990 US dollars, therefore, they have been translated to 2020 US dollars using a conversion factor of 1.98 [65].

The PROCESS code enables the usage of a Rankine cycle or an S-CO_2 Brayton cycle as the power cycle. If the inlet turbine temperature is provided as an input, the efficiency of the cycle is estimated following the correlation given by Dostal [66]. This efficiency is used to calculate the electric output of the system. In this case, as these values have already been calculated, the efficiency and the nominal electric output of the power plant are the given inputs.

The LCOE has been calculated from the costs provided by the PROCESS code and using the approach introduced in [67]:

$$LCOE = \frac{CC * CRF + \sum_x VC_x * CELF_x}{P_e} \tag{7}$$

Where CC is the total capital cost; CRF, the Capital Recovery Factor; VC_x and $CELF_x$, the variable cost and the Constant Escalation Levelization Factor for a certain item x and Pe, the energy produced during a year.

The CRF is calculated as a function of the discount rate (i) and the expected lifetime of the fusion power plant (n):

$$CRF = \frac{i * (1+i)^n}{(1+i)^n - 1} \tag{8}$$

The CELF takes into account the evolution of prices and costs during the lifetime of the plant:

$$CELF = \frac{k(1-k^n)}{1-k} * CRF \tag{9}$$

$$k = \frac{1+r_n}{1+i_{eff}} = \frac{1+r_n}{e^i - 1} \tag{10}$$

Where r_n is the nominal escalation rate and i_{eff}, the effective discount rate. r_n can be calculated from the real escalation rate (r_r) and from the inflation (r_i) as:

$$(1+r_n) = (1+r_r) * (1+r_i) \tag{11}$$

Table 8 contains the parameters used in the calculation of the LCOE (Table 9). The power plant lifetime, availability factor and discount rate have been obtained from the DEMO Baseline 2018. The real scaling rate of the auxiliary heating has been estimated through the cost increase of electricity in the European Union (EU27) in the 2016-2020 period using Eurostat data [68]. For the rest of the variable costs, a real scalation rate of 0 has been chosen. This is a conservative approach as most of them are expected to get cheaper as the technic and know-how increase. The inflation rate has been obtained from Eurostat data from the EU27 in the 2015-2020 period [68].

Table 8
DEMO Baseline 2018 economic parameters [65,68].

Discount rate (i)	0.065	Inflation rate (r_i)	0.0113
Real scalation rate aux. heating ($r_{i,heating}$)	-0.0022	**Life of the project**	40 years
Real scalation rate others ($r_{i,others}$)	0.0	**Availability factor**	75 %

Table 9
Results of the economic assessment.

	LCOE [$/MWh]	TOTAL COST [M$]
HLC.LDS	219.71	7419.70
HCL.LDS	227.48	7414.68
NC.LDS	231.49	7420.33
HLC.LDS-HT1	135.08	7336.30
HLC.LDS-HT2	120.62	7961.33
HLC.LDS-HT3	115.68	8244.83
SS-HLC.LDS	104.60	8269.93
SS-HLC.LDS-2T (800°C)	101.63	8277.36

Table 9 shows how the best way to decrease the LCOE is to improve the efficiency of the fusion power plant. Specially by increasing the maximum temperature of the system, the first three layouts of the table (HLC.LDS, HCL.LDS and NC.LDS) have a maximum operating temperature of 500°C while the rest can get up to 800°C. This temperature increase means a strong reduction in the LCOE of around 100$/MWh. Layouts HLC.LDS-HT1, HLC.LDS-HT2 and HLC.LDS-HT3 show the transition from a pulsed reaction to a steady-state system with decreasing dwell times and increasing pulse times; this shows the impact of more constant production and higher maximum temperature in the final price of the energy. Finally, the advanced steady-state layouts cut the LCOE by a third with respect to the low-temperature pulsed scenarios. Adding a second turbine to the system affects the LCOE by reducing it in ~3$/MWh.

The LCOE for the conservative cases that follow the DEMO Baseline 2018 show energy prices not unreasonably above the current trends of around 200$/MWh. It is reasonable to expect a significant drop in the prices as generations and expertise are built. In comparison, photovoltaic solar power cost was 350$/MWh in 2010; meanwhile, in 2016, the average prices dropped to ~140$/MWh [69]. With the increase of temperature (high-temperature layouts), the LCOE falls to the current electricity prices. These numbers are acceptable in the current energy market, especially after subsidies, as proposed in a similar study [70]. It is essential to highlight that the main goal of DEMO is not to achieve competitive energy prices but to be the first fusion reactor demonstrating the capabilities of a fusion power plant with net electricity production. Next generations of fusion power plants after DEMO will be built over the lessons learnt from ITER and DEMO with reduced cost as its main objective.

6. Conclusions

A framework has been developed to integrate the PROCESS code and the numerical solver EES to study the thermal and economic aspects of integrating different supercritical carbon dioxide cycle layouts with a fusion power plant. Fourteen layouts have been proposed and grouped into a more conservative (DEMO1, pulsed operation) and more advanced (DEMO2, steady-state operation) fusion reactors. The PROCESS code has been used to obtain the DEMO Baseline 2018, which defines the available power from each heat source and its boundary conditions.

A thermal storage system (TES) has been added to the twelve DEMO1 layouts to avoid standby times that would negatively affect the cycle. The sensitivity analysis of these layouts shows the importance of using the divertor (DIV) and shield (SHD) heat sources despite the constrain of the 150ºC temperature limit set by the cooling water. The optimum position for these two heat sources has been determined to be just after the low-temperature recuperator (LTR) at the high-pressure side, as it allows the recuperator to achieve a lower temperature at the low-pressure side. This analysis has also confirmed the efficiency increase of using a secondary compression after the LTR for the studied cases. The layout HLC.LDS, with a secondary compressor and a recuperator at the compressor outlet, is the most promising pulsed option with a 38% cycle efficiency. Comparing the electric efficiency results for the DEMO1 simulations with previous work shows good agreement with the obtained values, with efficiencies around 30-35%. The steady-state options achieve higher efficiencies (~55%), but are conditioned to the advancement of technology and plasma physics by the time of its construction. The study of intermediate scenarios between conservative DEMO Baseline 2018 and DEMO2 show that the maximum temperature of the power conversion system is the most relevant parameter. Rising the temperature from 500ºC to 800ºC increase the efficiency by more than 10%.

A significant part of the produced power is internally consumed by the reactor and the auxiliaries, meaning a 20% reduction of the plant efficiency. Reducing these consumptions will directly affect the viability of the plant and should be studied in future work. Additional reactor consumption may be necessary to sustain the steady-state scenario, which will affect the net power output. The temperature constraints on the divertor and shield coolant for DEMO1 also limit the cycle efficiency. Using helium or another cooling method instead of water will positively impact the cycle mean temperature, but it could increase the primary loop consumption. This possibility should be investigated to determine if the net change in plant efficiency is positive.

A TES system is an essential addition to a pulsed reactor (DEMO1) as it protects the machinery but at the cost of decreasing the fusion power plant efficiency. A phase-change material (PCM) system (molten salts) and a sensible heat storage one (solar salt plus water), have been proposed as possible candidates. However, further research needs to be carried out before PCM technologies get to the expected maturity level. For an S-CO_2 Brayton cycle, simulations of the effect of no TES system should be done to assess the fundamental importance of adding energy storage. Tritium recovery for the TES candidates should also be studied.

The PROCESS code has been used to assess the cost of the optimal layouts and their Levelized Cost of Electricity has been calculated. The economic analysis of DEMO1 type LDS layouts shows that this reactor is not economically competitive with the currently available energy producers. However, LCOE from high-temperature versions of DEMO1 can be below the range of current energy prices and, with the introduction of subsidies and support policies, could evolve positively in the energy market. DEMO2 scenarios show a significant decrease in its LCOE in comparison with today's electricity prices.

CRediT authorship contribution statement

J. Hidalgo-Salaverri: Conceptualization, Methodology, Software, Validation, Investigation, Resources, Writing – original draft, Visualization. **P. Cano-Megias:** Conceptualization, Methodology, Software, Investigation, Resources, Writing – review & editing, Visualization, Supervision. **R. Chacartegui:** Conceptualization, Methodology, Investigation, Resources, Writing – review & editing, Visualization, Supervision, Project administration. **J. Ayllon-Guerola:** Conceptualization, Investigation, Writing – review & editing, Supervision, Project administration. **E. Viezzer:** Conceptualization, Investigation, Writing – review & editing, Supervision, Project administration.

Declaration of Competing Interest

The authors declare that they have no known competing financial interests or personal relationships that could have appeared to influence the work reported in this paper.

Acknowledgements

The authors would like to thank J. Morris, M. Kovari and the rest of the PROCESS team of UKAEA for discussion and guidance on using the UKAEA systems code PROCESS for this work. The authors gratefully acknowledge the financial support of the Spanish Ministry of Science, Innovation and Universities (grant FPU17/06273), the H2020 Marie-Sklodowska Curie programme (grant agreement No. 708257) and the European Research Council (ERC) under the European Union's Horizon 2020 research and innovation programme (grant agreement No. 805162).

References

[1] T. Donné, European research roadmap to the realisation of fusion energy, EUROfusion (2018) https://www.euro-fusion.org/fileadmin/user_upload/EUROfusion/Documents/TopLevelRoadmap.pdf.
[2] L. Giancarli, V. Chuyanov, M. Abdou, M. Akiba, B.G. Hong, R. Lässer, C. Pan, Y. Strebkov, Breeding blanket modules testing in ITER: an international program on the way to DEMO, Fusion Eng. Des. 81A (2006) 393–405, https://doi.org/10.1016/j.fusengdes.2005.08.096.
[3] M. Kovari, C. Harrington, I. Jenkins, C. Kiely, Converting energy from fusion into useful forms, Fusion Eng. Des. 124 (2014) 10, https://doi.org/10.1177/0957650913514230.
[4] G. Federici, C. Bachmann, W. Biel, L. Boccaccini, F. Cismondi, S. Ciattaglia, M. Coleman, C. Day, E. Diegele, T. Franke, M. Grattarola, H. Hurzlmeier, A. Ibarra, A. Loving, F. Maviglia, B. Meszaros, C. Morlock, M. Rieth, M. Shannon, N. Taylor, M.Q. Tran, J.H. You, R. Wenninger, L. Zani, Overview of the design approach and prioritization of R&D activities towards an EU DEMO, Fusion Eng. Des. 109–111 (2016) 1464–1474, https://doi.org/10.1016/j.fusengdes.2015.11.050.
[5] S. Ishiyama, Y. Muto, Y. Kato, S. Nishio, T. Hayashi, Y. Nomoto, Study of steam, helium and supercritical CO2 turbine power generations in prototype fusion power reactor, Prog. Nucl. Energy. 50 (2008) 325–332, https://doi.org/10.1016/j.pnucene.2007.11.078.
[6] H. Zhao, G. Fukuda, R.P. Abbott, P.F. Peterson, H. Zhao, G. Fukuda, R.P. Abbott, P. F. Peterson, Optimized Helium-Brayton power conversion for fusion energy systems, 1055 (2017). https://doi.org/10.13182/FST05-A730.
[7] E.G. Feher, The supercritical thermodynamic power cycle, Energy Convers. 8 (1968) 85–90, https://doi.org/10.1016/0013-7480(68)90105-8.
[8] G. Sulzer, Verfahren zur erzeugung von arbeit aus warme, Swiss Pat. (1950), 269599.
[9] R. Chacartegui, J.M. Muñoz De Escalona, D. Sánchez, B. Monje, T. Sánchez, Alternative cycles based on carbon dioxide for central receiver solar power plants, Appl. Therm. Eng. 31 (2011) 872–879, https://doi.org/10.1016/j.applthermaleng.2010.11.008.
[10] C. Ortiz, R. Chacartegui, J.M. Valverde, A. Alovisio, J.A. Becerra, Power cycles integration in concentrated solar power plants with energy storage based on calcium looping, Energy Convers. Manag. 149 (2017) 815–829, https://doi.org/10.1016/j.enconman.2017.03.029.
[11] F. Crespi, D. Sánchez, J.M. Rodríguez, G. Gavagnin, Fundamental thermo-economic approach to selecting sCO2 power cycles for CSP applications, Energy Procedia 129 (2017) 963–970, https://doi.org/10.1016/j.egypro.2017.09.215.
[12] B.D. Iverson, T.M. Conboy, J.J. Pasch, A.M. Kruizenga, Supercritical CO2 Brayton cycles for solar-thermal energy, Appl. Energy. 111 (2013) 957–970, https://doi.org/10.1016/j.apenergy.2013.06.020.
[13] X. Wei, V. Manovic, D.P. Hanak, Techno-economic assessment of coal- or biomass-fired oxy-combustion power plants with supercritical carbon dioxide cycle, Energy Convers. Manag. 221 (2020), 113143, https://doi.org/10.1016/j.enconman.2020.113143.
[14] J. Zhou, M. Zhu, Y. Tang, K. Xu, S. Su, S. Hu, Y. Wang, J. Xu, L. He, J. Xiang, Innovative system configuration analysis and design principle study for different capacity supercritical carbon dioxide coal-fired power plant, Appl. Therm. Eng. 174 (2020), 115298, https://doi.org/10.1016/j.applthermaleng.2020.115298.
[15] F. Crespi, G. Gavagnin, D. Sánchez, G.S. Martínez, Supercritical carbon dioxide cycles for power generation: a review, Appl. Energy. 195 (2017) 152–183, https://doi.org/10.1016/j.apenergy.2017.02.048.
[16] P. Wu, Y. Ma, C. Gao, W. Liu, J. Shan, Y. Huang, J. Wang, D. Zhang, X. Ran, A review of research and development of supercritical carbon dioxide Brayton cycle technology in nuclear engineering applications, Nucl. Eng. Des. 368 (2020), 110767, https://doi.org/10.1016/j.nucengdes.2020.110767.
[17] J.I. Linares, L.E. Herranz, I. Fernández, A. Cantizano, B.Y. Moratilla, Supercritical CO2 Brayton power cycles for DEMO fusion reactor based on Helium Cooled Lithium Lead blanket, Appl. Therm. Eng. 76 (2015) 123–133, https://doi.org/10.1016/j.applthermaleng.2014.10.093.

[18] L. Vesely, V. Dostal, S. Entler, Study of the cooling systems with S-CO2 for the DEMO fusion power reactor, Fusion Eng. Des. 124 (2017) 244–247, https://doi.org/10.1016/j.fusengdes.2017.05.029.
[19] G. Federici, W. Biel, M.R. Gilbert, R. Kemp, N. Taylor, R. Wenninger, European DEMO design strategy and consequences for materials, Nucl. Fusion. 57 (2017) 92002, https://doi.org/10.1088/1741-4326/57/9/092002.
[20] S. Ushak, A.G. Fernández, M. Grageda, 3 - Using molten salts and other liquid sensible storage media in thermal energy storage (TES) systems, L.F.B.T.-A. in T.E. S.S. Cabeza. Woodhead Publ. Ser. Energy, Woodhead Publishing, 2015, pp. 49–63, https://doi.org/10.1533/9781782420965.1.49.
[21] A. Madhlopa, Principles of Solar Gas Turbines for Electricity Generation, 1st ed., Springer International Publishing, 2018.
[22] I. Sarbu, C. Sebarchievici, A comprehensive review of thermal energy storage, Sustain (2018) 10, https://doi.org/10.3390/su10010191.
[23] D.N. Nkwetta, F. Haghighat, Thermal energy storage with phase change material - A state-of-the art review, Sustain. Cities Soc. 10 (2014) 87–100, https://doi.org/10.1016/j.scs.2013.05.007.
[24] G. Besagni, L. Croci, Experimental study of a pilot-scale fin-and-tube phase change material storage, Appl. Therm. Eng. 160 (2019), 114089, https://doi.org/10.1016/j.applthermaleng.2019.114089.
[25] R. Chacartegui, A. Alovisio, C. Ortiz, J.M. Valverde, V. Verda, J.A. Becerra, Thermochemical energy storage of concentrated solar power by integration of the calcium looping process and a CO2 power cycle, Appl. Energy. 173 (2016) 589–605, https://doi.org/10.1016/j.apenergy.2016.04.053.
[26] A. Alovisio, R. Chacartegui, C. Ortiz, J.M. Valverde, V. Verda, Optimizing the CSP-calcium looping integration for thermochemical energy storage, Energy Convers. Manag 136 (2017) 85–98, https://doi.org/10.1016/j.enconman.2016.12.093.
[27] A. Gil, M. Medrano, I. Martorell, A. Lázaro, P. Dolado, B. Zalba, L.F. Cabeza, State of the art on high temperature thermal energy storage for power generation. Part 1-Concepts, materials and modellization, Renew. Sustain. Energy Rev. 14 (2010) 31–55, https://doi.org/10.1016/j.rser.2009.07.035.
[28] M. Kovari, R. Kemp, H. Lux, P. Knight, J. Morris, D.J. Ward, PROCESS ": A systems code for fusion power plants — Part 1 : Physics, Fusion Eng. Des. 89 (2014) 3054–3069, https://doi.org/10.1016/j.fusengdes.2014.09.018.
[29] M. Kovari, F. Fox, C. Harrington, R. Kembleton, P. Knight, H. Lux, J. Morris, PROCESS " : A systems code for fusion power plants – Part 2 : Engineering, Fusion Eng. Des. 104 (2016) 9–20, https://doi.org/10.1016/j.fusengdes.2016.01.007.
[30] S.A. Klein, Development and integration of an equation-solving program for engineering thermodynamics courses, Comput. Appl. Eng. Educ. 1 (1993) 265–275, https://doi.org/10.1002/cae.6180010310.
[31] M. Siccinio, W. Biel, M. Cavedon, E. Fable, G. Federici, F. Janky, H. Lux, F. Maviglia, J. Morris, F. Palermo, O. Sauter, F. Subba, H. Zohm, DEMO physics challenges beyond ITER, Fusion Eng. Des 156 (2020), 111603, https://doi.org/10.1016/j.fusengdes.2020.111603.
[32] G. Giruzzi, J.F. Artaud, M. Baruzzo, T. Bolzonella, E. Fable, L. Garzotti, I. Ivanova-Stanik, R. Kemp, D.B. King, M. Schneider, R. Stankiewicz, W. Stępniewski, P. Vincenzi, D. Ward, R. Zagórski, Modelling of pulsed and steady-state DEMO scenarios, Nucl. Fusion. (2015) 55, https://doi.org/10.1088/0029-5515/55/7/073002.
[33] G. Federici, R. Kemp, D. Ward, C. Bachmann, T. Franke, S. Gonzalez, C. Lowry, M. Gadomska, J. Harman, B. Meszaros, C. Morlock, F. Romanelli, R. Wenninger, Overview of EU DEMO design and R&D activities, Fusion Eng. Des. 89 (2014) 882–889, https://doi.org/10.1016/j.fusengdes.2014.01.070.
[34] J. Wesson, Tokamaks, 4th ed., Oxford University Press, 2011. Oxford.
[35] D. Maisonnier, I. Cook, S. Pierre, B. Lorenzo, D.P. Luigi, G. Luciano, N. Prachai, P. Aldo, DEMO and fusion power plant conceptual studies in Europe, Fusion Eng. Des. 81 (2006) 1123–1130, https://doi.org/10.1016/j.fusengdes.2005.08.055.
[36] D. Maisonnier, I. Cook, S. Pierre, B. Lorenzo, B. Edgar, B. Karin, D.P. Luigi, F. Robin, G. Luciano, H. Stephan, N. Claudio, N. Prachai, P. Aldo, T. Neill, W. David, The European power plant conceptual study, Fusion Eng. Des. 75–79 (2005) 1173–1179, https://doi.org/10.1016/j.fusengdes.2005.06.095.
[37] D. Maisonnier, I. Cook, P. Sardain, R. Andreani, L. Di Pace, R. Forrest, L. Giancarli, S. Hermsmeyer, P. Norajitra, N. Taylor, D. Ward, A Conceptual Study of Commercial Fusion Power Plants, 2005 https://www.euro-fusion.org/fileadmin/user_upload/Archive/wp-content/uploads/2012/01/PPCS_overall_report_final.pdf.
[38] G. Federici, C. Bachmann, L. Barucca, W. Biel, L. Boccaccini, R. Brown, C. Bustreo, S. Ciattaglia, F. Cismondi, M. Coleman, V. Corato, C. Day, E. Diegele, U. Fischer, T. Franke, C. Gliss, A. Ibarra, R. Kembleton, A. Loving, F. Maviglia, B. Meszaros, G. Pintsuk, N. Taylor, M.Q. Tran, C. Vorpahl, R. Wenninger, J.H. You, DEMO design activity in Europe: Progress and updates, Fusion Eng. Des 136 (2018) 729–741, https://doi.org/10.1016/j.fusengdes.2018.04.001.
[39] G. Federici, L. Boccaccini, F. Cismondi, M. Gasparotto, Y. Poitevin, I. Ricapito, An overview of the EU breeding blanket design strategy as an integral part of the DEMO design effort, Fusion Eng. Des. 141 (2019) 30–42, https://doi.org/10.1016/j.fusengdes.2019.01.141.
[40] L.V. Boccaccini, G. Aiello, J. Aubert, C. Bachmann, T. Barrett, A. Del Nevo, D. Demange, L. Forest, F. Hernandez, P. Norajitra, G. Porempovic, D. Rapisarda, P. Sardain, M. Utili, L. Vala, Objectives and status of EUROfusion DEMO blanket studies, Fusion Eng. Des. 109–111 (2016) 1199–1206, https://doi.org/10.1016/j.fusengdes.2015.12.054.
[41] H. Zohm, On the minimum size of demo, Fusion Sci. Technol. 58 (2010) 613–624, https://doi.org/10.13182/FST10-06.
[42] C. Harrington, Dynamic modelling of balance of plant systems for a pulsed DEMO power plant, Fusion Eng. Des. 98–99 (2015) 2147–2151, https://doi.org/10.1016/j.fusengdes.2015.03.029.
[43] J. Lucas, M. Cortés, P. Méndez, J. Hayward, D. Maisonnier, Energy storage system for a pulsed DEMO, Fusion Eng. Des. 82 (2007) 2752–2757, https://doi.org/10.1016/j.fusengdes.2007.03.007.
[44] E. Bubelis, W. Hering, Thermal Energy Storage System Proposal for DEMO Fusion Power Plant. Energy, Sci. Technol. 2015, Energy Conf. Sci. Res. Int. Conf. Exhib., Karlsruhe, Germany, 2015, 10.5445 /IR / 1000044290.
[45] M. Medrano, A. Gil, I. Martorell, X. Potau, L.F. Cabeza, State of the art on high-temperature thermal energy storage for power generation. Part 2-Case studies, Renew. Sustain. Energy Rev. 14 (2010) 56–72, https://doi.org/10.1016/j.rser.2009.07.036.
[46] C. Prieto, L.F. Cabeza, Thermal energy storage (TES) with phase change materials (PCM) in solar power plants (CSP). Concept and plant performance, Appl. Energy. 254 (2019), 113646, https://doi.org/10.1016/j.apenergy.2019.113646.
[47] A. Hauer, Z.A.E. Bayern, Storage Technology Issues and Opportunities, CERT Energy Storage Workshop, Paris, 2011 https://www.iea.org/events/workshop-on-energy-storage-issues-and-opportunities.
[48] J.I. Linares, E. Arenas, A. Cantizano, J. Porras, B.Y. Moratilla, M. Carmona, L. Batet, Sizing of a recuperative supercritical CO2Brayton cycle as power conversion system for DEMO fusion reactor based on Dual Coolant Lithium Lead blanket, Fusion Eng. Des. 134 (2018) 79–91, https://doi.org/10.1016/j.fusengdes.2018.06.026.
[49] M. Mehos, C. Turchi, J. Vidal, M. Wagner, Z. Ma, C. Ho, W. Kolb, C. Andraka, A. Kruizenga, Concentrating Solar Power Gen3 Demonstration Roadmap, Nrel/Tp-5500-67464. (2017) 1–140. https://doi.org/10.2172/1338899.
[50] J.I. Linares, A. Cantizano, E. Arenas, L. Batet, Y. Moratilla, Technical Report About Steady-State and Dynamic Analysis, EFDA, EUROfusion, 2014.
[51] J. Linares, A. Cantizano, B. Moratilla, L. Batet, Alternative range of viable secondary coolants and options for thermodynamic cycles, 2014.
[52] S.J. Zinkle, L.L. Snead, Designing radiation resistance in materials for fusion energy, Annu. Rev. Mater. Res. 44 (2014) 241–267, https://doi.org/10.1146/annurev-matsci-070813-113627.
[53] P.M. Raole, S.P. Deshpande, Structural materials for fusion reactors, Trans. Indian Inst. Met. 62 (2009) 105–111, https://doi.org/10.1007/s12666-009-0014-0.
[54] S.J. Zinkle, N.M. Ghoniem, Operating temperature windows for fusion reactor structural materials, Fusion Eng. Des. 51–52 (2000) 55–71, https://doi.org/10.1016/S0920-3796(00)00320-3.
[55] G.R. Romanoski, L.L. Snead, R.L. Klueh, D.T. Hoelzer, Development of an oxide dispersion strengthened, reduced-activation steel for fusion energy, J. Nucl. Mater. 283–287 (2000) 642–646, https://doi.org/10.1016/S0022-3115(00)00137-9.
[56] R.H. Jones, L.L. Snead, A. Kohyama, P. Fenici, Recent advances in the development of SiC/SiC as a fusion structural material, Fusion Eng. Des. 41 (1998) 15–24, https://doi.org/10.1016/S0920-3796(98)00285-3.
[57] J.I. Linares, A. Cantizano, E. Arenas, B.Y. Moratilla, V. Martín-Palacios, L. Batet, Recuperated versus single-recuperator re-compressed supercritical CO2Brayton power cycles for DEMO fusion reactor based on dual coolant lithium lead blanket, Energy 140 (2017) 307–317, https://doi.org/10.1016/j.energy.2017.08.105.
[58] R. Span, W. Wagner, A new equation of state for carbon dioxide covering the fluid region from the triple-point temperature to 1100 K at pressures up to 800 MPa, J. Phys. Chem. Ref. Data. 25 (1996) 1509–1596, https://doi.org/10.1063/1.555991.
[59] Z. Ma, G.C. Glatzmaier, C.F. Kutscher, Thermal energy storage and its potential applications in solar thermal power plants and electricity storage, in: ASME 2011 5th Int. Conf. Energy Sustain. ES 2011, 2011, pp. 447–456, https://doi.org/10.1115/ES2011-54077.
[60] Y. Ahn, S.J. Bae, M. Kim, S.K. Cho, S. Baik, J.I. Lee, J.E. Cha, Review of supercritical CO2 power cycle technology and current status of research and development, Nucl. Eng. Technol. 47 (2015) 647–661, https://doi.org/10.1016/j.net.2015.06.009.
[61] J.D. Galambos, STAR Code: Spherical Tokamak Analysis and Reactor Code, Unpubl. Intern. Oak Ridge Doc, 1990.
[62] P.J. Knight, M.D. Kovari, A User Guide to the PROCESS Fusion Reactor Systems Code, 2016 https://ccfe.ukaea.uk/wp-content/uploads/2019/11/A-User-Guide-to-the-PROCESS-systems-code.pdf.
[63] J. Sheffield, R.A. Dory, S.M. Cohn, J.G. Delene, L. Parsly, D.E.T.F. Ashby, W. T. Reiersen, Cost assessment of a generic magnetic fusion reactor, Fusion Technol 9 (1986) 199–249, https://doi.org/10.13182/FST9-2-199.
[64] R.L. Reid, J.D. Galambos, Architecture of the ETR [Experimental Test Reactor] Systems Code, United States, 1987 http://inis.iaea.org/search/search.aspx?orig_q=RN:20013830.
[65] U.S. Bureau of labor Statistics, Consumer Price Index, 2021 https://www.bls.gov/cpi/.
[66] P.H. Dostal, Vaclav; M.J. Driscoll, A Supercritical Carbon Dioxide Cycle for Next Generation Nuclear Reactors, 2004.
[67] A. Bejan, G. Tsatsaronis, M.J. Moran, Thermal Design and Optimization, John Wiley and Sons, 1996. New York [etc.
[68] Eurostat, Eurostat, 2021. (n.d.). https://ec.europa.eu/eurostat.
[69] IRENA, Rethinking Energy 2017, 2017. https://doi.org/10.1007/s00063-001-1014-y.
[70] S. Entler, J. Horacek, T. Dlouhy, V. Dostal, Approximation of the economy of fusion energy, Energy. 152 (2018) 489–497, https://doi.org/10.1016/j.energy.2018.03.130.